Combustion Theory and Modelling
Vol. 00, No. 00, Month 200x, 1–16

RESEARCH ARTICLE

Modeling of the subgrid scale wrinkling factor for large-eddy simulation of turbulent premixed combustion

Fabien Thiesset[a], Guillaume Maurice[a,b], Fabien Halter[a*] , Nicolas Mazellier[b], Christian Chauveau[a], Iskender Gökalp[a]

[a] *CNRS ICARE, Avenue de la Recherche Scientifique, 45072 Orléans Cedex 2 France*;
[b] *University of Orléans, INSA de Bourges, PRISME, EA 4229, 45072 Orléans, France*

(*v4.2 released October 2009*)

We propose a model for assessing the unresolved wrinkling factor in LES of turbulent premixed combustion. It relies essentially on a power-law dependence of the wrinkling factor to the filter size and an original expression for the 'active' corrugating strain rate. The latter is written as a product of an efficiency function which accounts for viscous effects and the kinematic constraint of Peters, by a recent expression for the turbulent strain intensity. Yields functional expressions for the fractal dimension and the inner cut-off length scale, the latter being *(i)* filter-size independent and *(ii)* consistent with the Damköhler asymptotic behaviours at both large and small Karlovitz numbers. A new expression for the wrinkling factor which incorporates finite Reynolds numbers effects is further proposed. Finally, the model is successfully assessed on an experimental filtered database.

Keywords: Large Eddy Simulation, Efficiency function, Flame wrinkling, Strain, Stretch

1. Introduction

Numerical simulation has become an extremely valuable tool for predicting turbulent reacting and non-reacting flows [1]. However, even though the progress in computing resources have been tremendous during the last decade or so, fully resolved simulations (Direct Numerical Simulations, DNS) still remain limited to some canonical configurations with relatively simple chemistry in simple geometries. One promising alternative is then to use Large Eddy Simulation (LES) that requires much less computer ressources and thus allow to tackle simulations of more complex geometries to face the challenges of the industry. The basic idea of LES is to explicitely calculate the large scales down to a cut-off length-scale (generally identified with the mesh size which is coarser than that of DNSs) while the contribution of the unresolved scales (in terms of i.e. momentum, energy, species transport, etc) is embedded into a so-called sub-grid scale (SGS) model. The computation quality and the results accuracy are inherently conditioned by the reliability of these SGS models [1].

As far as LES of turbulent reacting flows are concerned, several methods have been developped in the last decade, among these, the algebraic closure strategy is one of the most popular. The thickened flame approach [2, 3] is based on artificially

*Corresponding author. Email: fabien.halter@cnrs-orleans.fr

ISSN: 1364-7830 print/ISSN 1741-3559 online

DOI: 10.1080/13647830.YYYY.xxxxxx
http://www.tandfonline.com

thickenning the flame so that the flame thickness fits the mesh requirements of a LES. Such a procedure yields irremediably an attenuation in the flame wrinkling because the broadened flame acts as a filter on the turbulent eddies of similar size. This artifical decrease in flame wrinkling has thus to be modeled. The opposite approach is the G-equation [4, 5] procedure for which the flame is considered infinitely small compared to the mesh-size. The flame front is then described as a propagating surface tracked using a field variable called G (generally represented by a signed distance from the transported iso-surface). The SGS wrinkling of the G-field resulting from its interaction with SGS turbulent eddies is then accounted for through a SGS turbulent flame speed [4, 5]. Another strategy is the Filtered Tabulated Chemistry for LES (F-TACLES) [6] that takes advantage of the tabulated chemistry ability to handle complex chemistry. However, as for the two approaches mentioned above, the F-TACLES strategy also requires a model for the SGS wrinkling factor. This clearly demonstrates that independently of the strategy which is followed for tackling LES of turbulent combustion, there is systematically a need for efficient sub-grid scale wrinkling factor models.

Following the lines of Ref. [7], Colin et al. [2] and Charlette et al. [3] have developped a rather rigourous procedure for inferring the sub-grid scale wrinkling factor. The flame stretch (the rate of creation of surface aera) is then written as a turbulent strain (namely the unresolved turbulent velocity divided by the filter size) weighted by an efficiency function characterizing the transfer function between the turbulent strain and the flame stretch. This efficiency function is then evaluated by fitting the results of DNSs of a flame interacting with a pair of counter-rotating vortices. Although limited to 2D cases and simple chemistry, these computations incorporate explicitly finite rate chemistry, variable density and viscosity, curvature, straining, all these phenomena playing a significant role in the interaction between a vortex and a flame. More recently, a correction of previous efficiency functions [3] that accounts for the effect of Lewis number was further proposed in Ref. [8] using a similar approach.

As mentionned in Refs. [9, 10], although fundamentally relevant for understanding the basic mechanisms of flame folding due to the interaction with a vortex, it is worth stressing that flame-vortex interactions may not be representative of the processes at play in a turbulent flow. The reasons for this are twofold. Firstly, turbulence does differ from a toroïdal vortex in that sense that the latter does not experience vortex stretching, which is the essence of the energy cascade process from large to small scales [11]. Since vortex stretching is associated with the presence of larger scales with different orientations [11], flame-vortex interactions basically do not account for the collective effect between different vortex of different sizes. Consequently, the lifetime of a vortex pair is thus much more longer than that of similar size in a 3D turbulent flow. Secondly, a vortex pair has an inherent self induced convection velocity whereas a turbulent eddy of similar size experiences sweeping effects by much larger scales [12] and therefore convects at a much larger velocity. In other words, the convection velocity of a vortex-pair which is known for being responsible of flame surface creation [13], may differ significantly from that observed in a turbulent flow. Note however that these effects might possibly counterbalance each other since vortex stretching tends to decrease the vortex lifetime while sweeping effects leads to a larger convection velocity. Moreover, even though a single vortex may differ significantly from fully developped turbulence, their different dynamical aspects could also be hidden by some statistical operations (average) and finally lead to similar statistical behavior [14, 15].

The goal of the present paper is to propose a phenomenological scenario that allows to characterize flame stretching in a turbulent flow with the aim of de-

velopping a LES model for the SGS wrinkling factor. For this purpose, a similar formalism asa in Refs. [2, 3] is followed, i.e. the stretch of the flame is written as the product of the turbulent strain at a given scale by an efficiency function. However, instead of using DNS data of flame-vortex interaction, some physical statistical arguments are invoked for assessing the latter efficiency function and the local turbulent strain. These arguments rely essentially on some recent progress in the analytical description of turbulence that have been achieved mainly in the last decade. Then, we further proceed by proposing a LES model for the SGS wrinkling factor on the basis of a power-law distribution of wrinkling with filter-size [3, 16]. For this purpose, special care is given to the prediction of the inner cut-off, i.e. the smallest scale below which the flame front ceases being corrugated.

The paper is organized as follows. §2.1 aims at presenting the phenomenological analysis which leads to plausible analytical expressions for the turbulent strain, the efficiency function and hence the flame stretch. Then in §2.2, the LES model is presented and assessed in §3 from *a priori* tests using experiments in a turbulent Bunsen Burner. Conclusions are finally drawn in §4.

2. Presentation of the model

2.1 *Active stretch rate*

The key ingredient for modeling the SGS wrinkling factor is the rate of strain which is known to be partly responsible for the corrugation of the flame front [2, 3, 7, 16–18]. Since turbulence gives rise to a wide and continuous range of scales, it is essential to tackle a 'local' description, i.e. by assessing the contribution of each scale r to the fluctuating quantity under consideration. Such a scale-by-scale description can be carried out in either spectral space using Fourier transforms or in physical space by means of either correlation or structure functions. Similar treatments apply for any turbulent quantity, especially the one of interest here, i.e. the rate of strain. In a recent paper [19], an expression for the contribution of a given scale r to the strain intensity $\mathcal{S}$ was derived (hereafter r denotes either a typical turbulent scale or the LES filter size). In a locally isotropic context, in Kolmogorov units (indicated by an asterisk), the local strain rate reads [19]

$$\mathcal{S}(r^*) = \left[\frac{1}{r^*}\frac{\partial}{\partial r^*}\left\langle(\Delta q^*)^2\right\rangle + \frac{1}{2}\frac{\partial^2}{\partial r^{*2}}\left\langle(\Delta q^*)^2\right\rangle\right]^{1/2}. \tag{1}$$

$r^* \equiv r/\eta$ and $\left\langle(\Delta q^*)^2\right\rangle \equiv \left\langle(\Delta q)^2\right\rangle/u_K^2$ where the Kolmogorov scales are $\eta = (\nu^3/\epsilon)^{1/4}$ and $u_K = (\nu\epsilon)^{1/4}$, ϵ being the mean kinetic energy dissipation rate and ν the kinematic viscosity. $\left\langle(\Delta q)^2\right\rangle = \langle\Delta u_i \Delta u_i\rangle$ (summation convention applies to double Roman indices) is generally interpreted as the total kinetic energy at a given scale. $\Delta\bullet = \bullet(x+r) - \bullet(x)$ is the spatial increment of the quantity $\bullet$ between two points separated by a distance r. The brackets stands for a suitable average. The full derivation of Eq. (1) is not recalled here but the reader can refer to Ref. [19] where the derivation of the general (anisotropic) expression together with the simplified (isotropic) relation for $\mathcal{S}(r)$ is described in detail. The rate of strain thus appears related to the Laplacian (here expressed in spherical coordinates thanks to local isotropy) of the total kinetic energy at a given scale $\left\langle(\Delta q^*)^2\right\rangle$. As the scale r decreases, the rate of strain monotically increases towards the Kolmogorov strain u_K/η, whilst it is zero at large scales. The transport equation for $\left\langle(\Delta q^*)^2\right\rangle$ which follows from an extension of the pioneering work in Refs. [20, 21] to slightly

inhomogeneous locally isotropic flows writes [22]

$$\mathcal{I}^* - \frac{3}{4r^*}\left\langle \Delta u^* (\Delta q^{*2}) \right\rangle + \frac{3}{2r^*}\frac{\partial \left\langle (\Delta q^*)^2 \right\rangle}{\partial r^*} = 1. \tag{2}$$

Eq. (2) describes the statistical equilibrium between the different ranges of turbulent scales. The first term on LHS of Eq. (2) corresponds to the injection of kinetic energy at large scales through the combined effect of advection, production, turbulent or pressure diffusion. The energy then cascades towards smaller scales in an intermediate range of scales (the inertial range), this process being characterized by the second term on LHS of Eq. (2). Finally, the last term (hereafter formally written as $\mathcal{V}$) stands for the loss of energy by viscous effects and predominates at the smallest eddies. Remarkable is the fact that the expression for the viscous term appears in the expression for $\mathcal{S}$. Furthermore, at the smallest scales, it is readily shown that

$$\lim_{r^*\to 0} \mathcal{S}^2(r^*) = \lim_{r^*\to 0} \mathcal{V}(r^*) = 1. \tag{3}$$

This indicates that at the smallest scales, all the strain contributes to viscous dissipation and will thus not be efficient enough to corrugate the flame front. In addition to viscous effects, Ref. [23] suggested that there might be also a kinematic constraint that precludes scales r with characteristic velocity U_r (to be defined later) smaller than the laminar flame speed S_L from wrinkling the flame front. These two key ingredients (viscous + kinematic constraint) naturally lead us to a new definition for the active corrugating stretch rate $\mathcal{K}$ (the rate of creation of flame surface), viz.

$$\mathcal{K}(r^*) = \mathcal{C}(r^*)\mathcal{S}(r^*) = \mathcal{C}_1(r^*)\mathcal{C}_2(r^*)\mathcal{S}(r^*) \tag{4a}$$

$$\mathcal{C}_1(r^*) = 1 - \mathcal{V}(r^*) \tag{4b}$$

$$\mathcal{C}_2(r^*) = \frac{1}{2}\left\{1 + \mathrm{erf}\left[3\log\left(\frac{U_r}{S_L}\right)\right]\right\} \tag{4c}$$

Few comments have to be drawn at this stage.

(i) As in Refs. [2, 3, 7], the 'active' stretch rate of the flame is written as the product between the turbulent strain rate and an efficiency function (or transfer function) which characterizes the efficiency of a given turbulent eddy r with strain $\mathcal{S}(r)$ to stretch the flame front. The effect of curvature which also contributes to the flame stretch is taken into account in an implicit manner through the latter efficiency function.

(ii) The efficiency function $\mathcal{C}_1(r^*)$ (Eq. (4b)) accounts for the rate of strain whose intensity is large enough compared to viscous effects for effectively corrugating the flame front. At large scales, $\mathcal{C}_1(r^*) \to 1$ whereas as $r^* \to 0$, $\mathcal{C}_1(r^*) \to 0$, as expected.

(iii) On the other hand, the second efficiency function $\mathcal{C}_2(r^*)$ (Eq. (4c)) whose formulation is similar to Ref. [3], is the kinematic constraint which follows from the suggestion of Ref. [23]. As mentionned by Ref. [23], the kinematic restoration mechanism acts in damping the flame wrinkling through the burning of fresh gas pockets of curvature $\sim 1/r$ at a speed S_L. Hence, the function $\mathcal{C}_2(r^*)$ describes basically the effect of curvature on the flame stretch.

(iv) It is worth recalling that unlike previous studies [2, 3, 7, 17] for which $\mathcal{C}$ was

assessed by means of canonical DNSs of flame vortex interactions, a plausible phenomenological interpretation of this efficiency function is provided in the present case.

At this stage, a rather realistic functional for $\overline{(\Delta q^*)^2}$ and U_r needs to be further employed for an analytical expression for $\mathcal{K}(r^*)$ to be derived. In previous efforts [2, 3, 7, 9, 16, 17, 23], inertial range relations were used for describing $\overline{(\Delta q^*)^2}$ and U_r, i.e. $\overline{(\Delta q^*)^2} \propto U_r^2 \propto r^{2/3}$. Clearly, such an hypothesis might not be applicable since the Reynolds numbers generally encountered in practical situations is not sufficiently large for the inertial range to be discernible. Furthermore, the latter inertial range relation is in essence viscosity-independent whereas the viscous cut-off of energy spectra or structure functions at small scales might play a significant role as far as interactions with the flame front are concerned.

In order to provide a more appropriate expression for both $\left\langle (\Delta q^*)^2 \right\rangle$ and U_r which accounts for finite Reynolds number effects and viscous cut-off, we first recall that in the dissipative range, under the constraint of local isotropy, we have $\left\langle (\Delta q^*)^2 \right\rangle = r^{*2}/3$. In the inertial range, the Kolmorogov's relation reads $\left\langle (\Delta q^*)^2 \right\rangle = C_q r^{*2/3}$ (C_q is related to the Kolmogorov constant C_u by $C_q = 11C_u/3$ and will hereafter be set to $22/3$ provided $C_u = 2$ [24]). Finally, at large scales $\left\langle (\Delta q^*)^2 \right\rangle = 2\left\langle q^{*2} \right\rangle$, where $\left\langle q^{*2} \right\rangle$ is related to the turbulent Reynolds number $Re_t = u' L_t/\nu$ (L_t is the integral length-scale and u' a typical velocity fluctuation) through the relation $\left\langle q^{*2} \right\rangle = 3Re_t^{1/2}$. Hereafter, a value of 300 for $\left\langle q^{*2} \right\rangle$ is prescribed as an illustration. Following an elegant interpolation first proposed by Batchelor [25], these asymptotic scalings can be matched together in a parametric equation of the form [24, 26, 27]

$$\left\langle (\Delta q^*)^2 \right\rangle = \frac{r^{*2}}{3} \left[1 + \left(\frac{r^*}{r_1^*} \right)^2 \right]^{-2/3} \left[1 + \left(\frac{r^*}{r_2^*} \right)^2 \right]^{-1/3} \tag{5}$$

where $r_1^* = (3C_q)^{3/4}$ is the cross over between the viscous and inertial range, whilst the cross-over between large and inertial scales is given by $r_2^* = (2\overline{q^{*2}}/C_q)^{3/2}$. Eq. (5) is the analogous in physical space of some existing parametric expression for kinetic energy distribution in spectral space (the Pope's [28] or Pao's [29] energy spectra for instance). Even though this parametric expression is built using asymptotic relations, it appears to be well suited for describing $\left\langle (\Delta q^*)^2 \right\rangle$ even at low Reynolds numbers [24]. Then, since under the assumption of homogenity and isotropy,

$$\lim_{r \to \infty} \left\langle (\Delta q^*)^2 \right\rangle = 2 \left\langle \Delta q^{*2} \right\rangle = 6 \left\langle u^2 \right\rangle / u_K^2 \tag{6}$$

one can define U_r as

$$\frac{U_r}{S_L} = \left[\frac{\left\langle (\Delta q^*)^2 \right\rangle}{6} \right]^{1/2} Ka^{1/2}. \tag{7}$$

so that $U_r/S_L \to u'/S_L$ as $r \to \infty$. The Karlovitz number Ka is defined as $Ka = (u_K/S_L)^2 = (\delta_L/\eta)^2$ where $\delta_L = D/S_L$ is the laminar flame thickness, with D the fresh gas thermal diffusivity. It is worth noting that this expression for U_r might be preferably used to construct spectral diagram following the lines of Ref. [9] because it accounts for finite Reynolds number effects and viscous cut-off. By further using

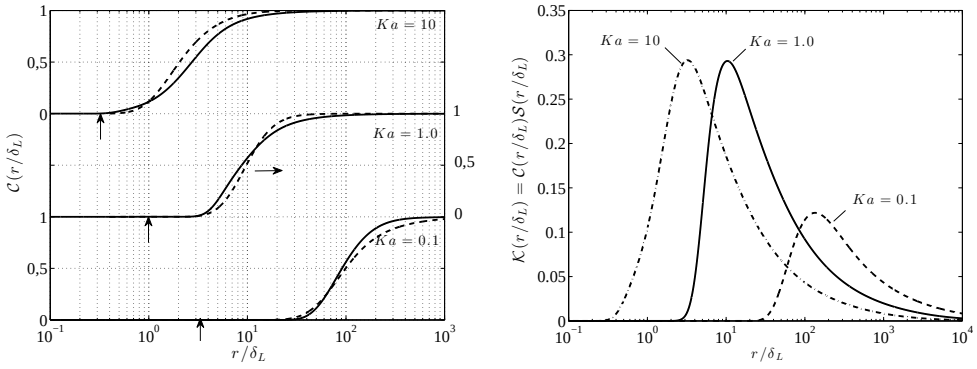

(a) (b)

Figure 1. (a) Comparison of the proposed efficiency function (—) $\mathcal{C}(r/\delta_L)$ as a function of filter size r/δ_L with that of Ref. [3] (- - -). Vertical arrows stand for η/δ_L. (b) Effective rate of stretch $\mathcal{C}(r/\delta_L)\mathcal{S}(r/\delta_L)$ for three different Karlovitz numbers, - - - $Ka = 0.1$; — $Ka = 1.0$; – · – $Ka = 10$.

Eq. (5) yields analytical expression for $\mathcal{V}$, $\mathcal{S}$, and hence $\mathcal{K}$

$$\mathcal{V}(r^*) = \frac{3\left\langle(\Delta q^*)^2\right\rangle}{r^{*2}}\left[1 - B\right], \tag{8a}$$

$$\mathcal{S}^2(r^*) = \frac{2\left\langle(\Delta q^*)^2\right\rangle}{r^{*2}}\left[3\left(2B_1^2 + B_2^2\right) + (1-B)\left(\frac{5}{2} - B\right) - 1\right], \tag{8b}$$

$$B_1 = \frac{1}{3}\left(\frac{r^*}{r_1^*}\right)^2\left[1 + \left(\frac{r^*}{r_1^*}\right)^2\right]^{-1}, \tag{8c}$$

$$B_2 = \frac{1}{3}\left(\frac{r^*}{r_2^*}\right)^2\left[1 + \left(\frac{r^*}{r_2^*}\right)^2\right]^{-1}, \tag{8d}$$

and $B = 2B_1 + B_2$.

The proposed efficiency function $\mathcal{C}(r) = \mathcal{C}_1(r)\mathcal{C}_2(r)$ is compared to that of Ref. [3] which writes

$$\mathcal{C}_{ch} = \frac{1}{4}\left\{1 + \mathrm{erf}\left[0.6\log\left(\frac{r}{\delta_L^{ch}}\right) - \left(\frac{U_r}{S_L}\right)^{-1/2}\right]\right\}\left\{1 + \mathrm{erf}\left[3\log\left(\frac{U_r}{S_L}\right)\right]\right\}. \tag{9}$$

The latter expression is an extension of the DNS based expression provided in Ref. [2] to account for the kinematic constraint discussed previously. To plot $\mathcal{C}_{ch}$, use was made of Eq. (7) for U_r. For comparing $\mathcal{C}$ and $\mathcal{C}_{ch}$, special care has been paid in using a similar definition for the laminar flame thickness. More precisely, Ref. [2] used a value for δ_L^{ch} for the flame thickness that was 3.7 times larger than δ_L. Results are presented in Fig. 1(a). As the Karlovitz number increases, both expressions progressively drift towards smaller r/δ_L, as expected from the decreasing ratio between δ_L and the Kolmogorov length-scale η. Note that at low Karlovitz number, the efficiency function tends to zero at scales larger than η (denoted by vertical arrows) revealing that the kinematic constraint $\mathcal{C}_2$ predominates by comparison with $\mathcal{C}_1$. At high Karlovitz numbers, the opposite is observed indicating that viscous effects are mostly perceptible. Departures between $\mathcal{C}$ and $\mathcal{C}_{ch}$ are globally rather small. Hence, this provides strong support in favour of the present phenomenological approach for estimating the efficiency function.

The active stretch rate for Karlovitz number of 0.1, 1.0 and 10 is displayed in Fig. 1(b). At low Karlovitz number ($\eta < \delta_L$), the stretch is active at rather large-scales whilst it drifts towards smaller scales as Ka increases. The maximum value of $\mathcal{K}$ is significantly reduced at low Karlovitz number as a consequence of the kinematic constraint which does not allow scales with characteristic velocity smaller than S_L to exist. Remarkable is the maximum magnitude of the Kolmogorov normalized rate of stretch at high Karlovitz numbers which is about 0.29, this value being extremely close to the one acting on a material surface found by both Ref. [30] and Ref. [31] from DNSs. Interestingly, this suggests that, ignoring heat release, the flame behaves as a passive interface for high Karlovitz numbers $Ka > 1$.

To summarize, it turns out that the phenomenological analysis provided here allows to quantify the transfer function $\mathcal{C}$ between flame stretch and turbulent strain with a reasonnable degree of agreement with DNSs of flame-vortex interactions. This was unexpected *a priori* given the substancial difference in the approaches but provides support for the conceptual bridge that can be built between canonical flame-vortex interactions and fully developped turbulent reacting flows. In the following, these results will be used with the aim of proposing a model for the SGS wrinkling factor.

2.2 *Inner-cut off and wrinkling factor*

There is wealth of experimental [32, 33], numerical [16, 18, 34] and analytical [35–37] support in favour of fractal concepts for describing the multi-scale distribution of flame folding in turbulent premixed combustion. Namely, following a (mono-) fractal approach, the SGS wrinkling factor Ξ (the ratio of the total to the resolved flame surface density), or equivalently the normalized SGS reactants consumption speed S_T/S_L is assumed to follow a power-law (sometimes referred to as fractal) dependence with r of the form

$$\Xi = \frac{S_T}{S_L} = \left[1 + \left(\frac{r}{\eta_i}\right)\right]^{\beta}, \tag{10}$$

where $\beta = D_f - 2$ with D_f the fractal dimension and η_i the inner cut-off, i.e. the smallest characteristic length scale of the flame front wrinkling. Eq. (10) suggests that $\Xi \to 1$ for $r \ll \eta_i$ (i.e. the flame surface density is fully resolved for filter sizes smaller than η_i), and that $\Xi = (r/\eta_i)^{\beta}$ for scales much larger than η_i (i.e. the wrinkling factor follows a power-law variation with filter size). However, it can be readily shown that $\Xi \to \infty$ as $r \to \infty$. This appears to be rather non physical as it is well known that there exists an outer cut-off η_o beyond which the wrinkling factor reaches a constant value. To account for this, we extend Eq. (10) through an additional term, viz.

$$\Xi = \frac{S_T}{S_L} = \left[1 + \left(\frac{r}{\eta_i}\right)^{\alpha}\right]^{\beta/\alpha} \left[1 + \left(\frac{r}{\eta_o}\right)^{\alpha}\right]^{-\beta/\alpha} \tag{11}$$

so that Ξ reaches a plateau as $r \to \infty$. The exponent α is introduced here for the sake of generality. Pragmatically speaking, α describes the sharpness of the transition between the 3 following different scalings *(i)* for $r \ll \eta_i$, $\Xi = 1$, *(ii)* for $\eta_i \ll r \ll \eta_o$, $\Xi \propto r^{\beta}$ and *(iii)* for $r \gg \eta_o$, $\Xi = (\eta_o/\eta_i)^{\beta}$. Whilst previous fractal models for the wrinkling factor [2, 3, 16, 18] generally use a value of 1 for α and

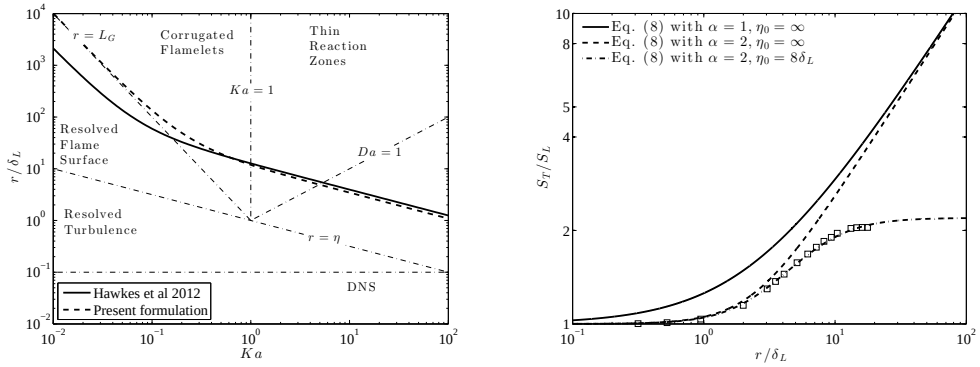

(a) (b)

Figure 2. (a) Inner cut-off length-scale η_i in the LES regime diagram [4]. - - - corresponds to the present formulation, viz. $N = 1$, $a = 1$ and $b = r_1^*$ and — $N = 4$, $a = 0.2$ and $b = 12.5$ (Ref. [16]). (b) S_T/S_L as a function of filter size r/δ_L. □ DNS data of Ref. [16] which are compared to that modeled by Eq. (11) with η_i and β predicted using $N = 1$, $a = 1$ and $b = r_1^*$. — $\alpha = 1, \eta_o = \infty$, - - - $\alpha = 2, \eta_o = \infty$, – · – $\alpha = 2, \eta_o/\delta_L = 8$. For all curves, the Karlovitz number was set to $Ka = 11$.

supposes $\eta_o \propto r$ (so that the rightmost term of Eq. (11) vanishes consistently with Eq. (10)), no particular prediction can be drawn at this stage. This point will be examined later when results are compared to some DNS data. Eq. (11) for the wrinkling factor is conjectured here but further work is needed for demonstrating its existence on some analytical basis.

To further proceed, we now have to relate the inner cut-off length-scale η_i to the rate of stretch at a given scale. Generally [2, 3, 16–18], η_i is inferred from a dynamical equilibrium hypothesis between production and destruction of SGS flame surface density. Here, we propose an alternative approach, conjecturing that η_i can be identified with the scale r at which the effective turbulent stretch rate $\mathcal{K}(r)$ is maximum, i.e. $\eta_i \equiv r$ such as $\mathcal{K}(r) = \max[\mathcal{K}(r)]$. We may justify this choice by arguing that the scale η_i at which $\mathcal{K}$ is maximum corresponds to the scale at which the stretch characteristic time scale is the smallest by comparison with the viscous (i.e. the Kolmogorov time scale) characteristic time scale. We can further justify the latter choice by arguing that the distribution of $\mathcal{K}(r)$ can be interpreted as a dispersion relation, i.e. the flame aera A increases as $A(t) = \exp(\mathcal{K}(r)t)$ with time [7, 30, 31, 38]. Therefore, the most amplified (or probable) scale will be that corresponding to the maximum of stretch. The maximum value of $\mathcal{K}$ at high Karlovitz number which is consistent with the estimation of both Ref. [30] and Ref. [31] also encourages us in adopting this definition for η_i. Finally, a practical advantage of using this definition is that the inner-cut off length-scale then remains filter size independent (in agreement with the DNS result of Ref. [16], see Fig. 11) and it is characteristic of a physical rather than a numerical quantity, following the suggestion of Ref. [16].

Results are presented in Fig. 2(a), where η_i/δ_L is plotted as a function of the Karlovitz number. Note that the derivation of an exact expression for η_i (scale at which the effective stretch rate is maximum) is not obvious. Instead, η_i has been estimated by searching the zero crossing of $\partial\mathcal{K}/\partial r$. Then, the evolution of η_i has been fitted with an appropriate functional built on relevant flame and/or turbulence parameters. Noticeable is the transition between two different regimes at low and high Karlovitz number which appears at $Ka \approx \{0.1 - 1\}$. At low Karlovitz numbers, $\eta_i/\delta_L \propto Ka^{-2}$, meaning that η_i is proportional to the Gibson length-scale [23] L_G . On the other hand, it appears that at high Karlovitz, $\eta_i/\delta_L = r_1^* Ka^{-1/2}$, i.e. is equal to the cross-over length-scale between the viscous and inertial range

introduced previously (Eq. (5)). It is worth recalling that the latter expression for η_i has already been proposed in Ref. [39]. There is thus a transition between two regimes, the first one at low Karlovitz numbers where the kinematic constraint $\mathcal{C}_2$ dominates (as noted in Fig. 1(a)) and the inner cut-off scales with the Gibson length-scale. For this range of Karlovitz numbers, the flame front is a highly active scalar, whose propagation speed acts as a filter precluding fresh gas pockets with characteristic scales smaller than L_G to exist. The second regime, at large Karlovitz number, indicates that the cut-off scale is proportional to η (or similarly the Obukhov-Corrsin length-scale notwithstanding the constancy of the Schmidt number). In this regime, the flame front thus behaves rather like a passive scalar [16]. These two different regimes corresponds respectively to the Damkhöler large-scale and small-scale asymptotic limits as discussed in Ref. [4] and further recovered analytically in Ref. [16] on the basis of both dimensional and dynamical arguments. Ref. [16] further proposed the following functional to "smoothly" interpolate these two regimes in a single expression, viz.

$$\frac{\eta_i}{\delta_L} = \left[\left(aKa^{-2}\right)^N + \left(bKa^{-1/2}\right)^N \right]^{1/N}. \tag{12}$$

The magnitude of N characterizes the sharpness of the transition (a value of 4 was chosen in Ref. [16]), and $a = 0.2$, $b = 5.5Sc^{-3/4} \approx 12.5$ (providing a Schmidt number $Sc = \nu/D$ of 0.335 for the hydrogen-air mixture at an equivalence ratio of 0.7 and a temperature of 700K as per Ref. [16]) were set *ad hoc* in Ref. [16]. Our analytical approach allows to derive the constants a, b, N of Eq. (12) which appear to be $a = 1$, $b = r_1^*$ and $N = 1$. Unlike Ref. [18] for which an empirical expression for β was employed, Ref. [16] demonstrated that the fractal dimension D_f should transit from a value of 7/3 at low Karlovitz number corresponding to the fractal dimension of a turbulent/non turbulent interface, to a value of 8/3 at high Karlovitz numbers, the latter value being generally observed for passive scalar fields in fully turbulent flows. To characterize this transition, Ref. [16] proposed the following parametric relation

$$\beta = D_f - 2 = \frac{1}{3} + \frac{1}{3}\frac{\left(bKa^{-1/2}\right)^N}{\left(aKa^{-2}\right)^N + \left(bKa^{-1/2}\right)^N}. \tag{13}$$

Plugging the prediction for η_i and β as given by Eqs. (12) and (13) into Eq. (11) yields an estimation of the sub-grid scale wrinkling factor Ξ or identically S_T/S_L as a function of filter size r and Karlovitz number. Results are presented in Fig. 2(b). When compared to the DNS results of Ref. [16] (see Fig. 2(b)), it is observed that, keeping η_i and β unchanged, a value of 2 for α and $\eta_o/\delta_L = 8$ (i.e. about three times larger than the integral length-scale) are much more suitable. Speculatively, the fact that a value of 2 for α appears more appropriate suggests that the fractal facet of turbulent flames is most likely related to its surface (i.e. r^2) rather than to its scale (r^1). At this stage, we have to emphasize that the parameters $\beta = D_f - 2$ and η_i are kept constant to obtain the curves in Fig. 2(b), whereas the apparent slope in the 'inertial' range of filter size appears less steeper in the DNS. This indicates that in most of practical situations, the scale separation between η_o and η_i (or equivalently the turbulent Reynolds number) is not sufficiently large for a proper fractal dimension to be unambiguously inferred and its estimation is clearly biased by some so-called finite Reynolds number effects [40]. Consequently, finite Reynolds number effects are likely to shed doubts on most of the experimental or

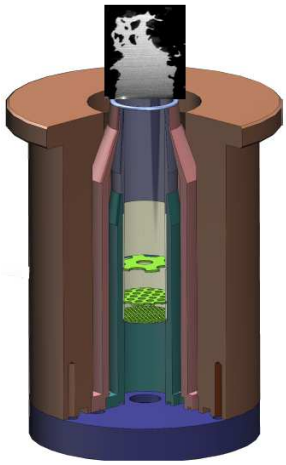

Figure 3. High-pressure Bunsen burner with the multi-grid injection system used in the present study. Also displayed a typical tomography image obtained for the case Ka^+

Case	Pressure	ϕ	S_L	δ_L	u'/S_L	L_t/δ_L	Ka	Re_t
-	[MPa]	-	[m.s^{-1}]	[mm]	-	-	-	-
Ka^+	0.3	0.6	0.058	0.127	14-6	33-50	6.3-1.4	660-430
Ka^-	0.1	0.8	0.227	0.083	3.6-2	51-65	0.95-0.36	230-160

Table 1. Flame and flow parameters for case Ka^+ and Ka^-.

numerical estimations of β and η_i and the quest for an universal value or universal evolution is worth being revisited.

To conclude about the model, it turns out that the only input of the model are the Karlovitz number and the integral length-scale that ought to be updated locally and at each time-step in a LES. Then, the inner cutoff and fractal dimension are evaluated according to Eq. (12) and (13) respectively. Finally, once η_i and β are known, the wrinkling factor is computed through Eq. (11) and the total flame surface density is recovered by multiplying the resolved flame surface density by Ξ.

3. A priori tests using experiments

To further validate the reliability of the present model, *a priori* tests are provided by comparing to experiments in a high pressure Bunsen Burner. The experimental set-up has been fully detailed in Refs. [41, 42] and references therein and is briefly recalled here.

3.1 *Experimental setup*

The Bunsen burner (see Fig. 3) has a diameter of 25mm and is placed in a chamber of inner diameter 300mm and height 1350mm that allows to reach pressure magnitudes up to 0.5 MPa. Intense turbulence is generated by a multi-scale grid system (see Fig. 3) which has been fully characterized by means of Laser Doppler and hot-wire Velocimetry in Ref. [41].

Two different methane-air mixtures at two different pressure are investigated for these tests. These two cases were chosen such as to correspond roughly to the high and low Karlovitz regimes discussed previously. Flame and flow parameters

are summarized in Table 1. For the first case, hereafter denoted as case Ka^+, the pressure in the chamber is 0.3MPa and the mixture equivalence ratio ϕ is 0.6. The second case, hereafter denoted as case Ka^-, is at 0.1MPa and equivalence ratio of 0.8. For the two cases the mixture inlet velocity is set to 3.6m.s^{-1}. The laminar flame speed and thickness have been calculated using the PREMIX code [43] and the CHEMKIN-II [44] database together with the GRI-Mech [45] ver.3.0 mechanism. We found $S_L = 0.058$m.s^{-1} and $\delta_L = D/S_L = 0.127$mm for case Ka^+ and $S_L = 0.227$m.s^{-1} and $\delta_L = 0.083$mm for case Ka^-. For case Ka^+, the ratio between turbulence intensity (on the centerline of the jet) and laminar flame speed is decreasing between 14 at the burner inlet to 6 at downstream location where the mean progress variable was 5% (hereafter this position will be denoted H_f). For case Ka^-, this ratio varies between 3.6 and 2. Because of the inhomogeneity in the streamwize direction (transverse inhomogeneity was found to be much smaller), local downstream values for the Karlovitz number $Ka(x)$ were used for calculating Ξ. The Karlovitz number has been calculated by $Ka(x) = (\delta_L/\eta(x))^2$. Use was made of the isotropic (1D) surrogate for $\epsilon(x)$ and hence $\eta(x)$. It was found that the Karlovitz number was decreasing between 6.3 at the burner exit to 1.4 at a downstream location $x = H_f$ for case Ka^+. For case Ka^-, $0.95 < Ka < 0.36$. The integral length-scale L_t calculated through the correlation function increases between 4.2 to 6.4mm as one travels downstream in the burner.

Measurements are carried out by means of High-speed Mie-scattering tomography using a Phantom V1210 camera working at an acquisition rate of 10kHz, and a continuous Coherent Verdi G20 Laser. The spatial resolution is $dx = 0.105$mm. Seeding of the flow is made with organic oil droplets with typical size of about 1μm which vaporize around 300°C. The instantaneous flame front corresponding to the iso-temperature at which the olive oil droplets totally vaporize, is tracked by standard contour edge detection. Yields the progress variable c field, which is by definition equal to 0 and 1 in the unburned and burned gas respectively.

It is worth stressing that there might be a limitation in the model as far as high Karlovitz numbers are concerned. Indeed, in this regime, the flamelet hypothesis might break down so that the wrinkling factor may depend on the progress variable. One solution then consists in conditionning the flame surface density by the iso-c of the reaction zone, which remains intact even in the broadened flame regime. The main difficulty will be then to model the effect of turbulence on the consumption speed which appears in the expression of the total heat release. However, as demonstrated by Hawkes et al. [46] algebraic models remain appropriate even for Karlovitz number of the order of 10. We are thus optimistic about the relevance of testing the model for the case Ka^+.

3.2 *Comparison with experiments*

We followed the same method as Ref. [47] for measuring the flame surface density. The Reynolds averaged Flame Surface Density (FSD) is thus calculated through $\langle|\nabla c|\rangle$, whilst the resolved surface density is $\langle|\nabla \overline{c}|\rangle$, where c is the progress variable and the overbar stands for filtered quantities using a (Reynolds) gaussian filter. Then, the total FSD is reconstructed by multiplying $\langle|\nabla \overline{c}|\rangle$ by the wrinkling factor $\Xi(x)$ as given by Eq. (11) with $Ka(x)$ as an input. Since measurements are made by tomography, only 2D flame surface density can be inferred. There have been many studies [46–49] dedicated to the correction factors that have to be applied for assessing 3D flame surface density from 2D measurements. Here, for testing the present model, we assume that the later correction factor is the same for both

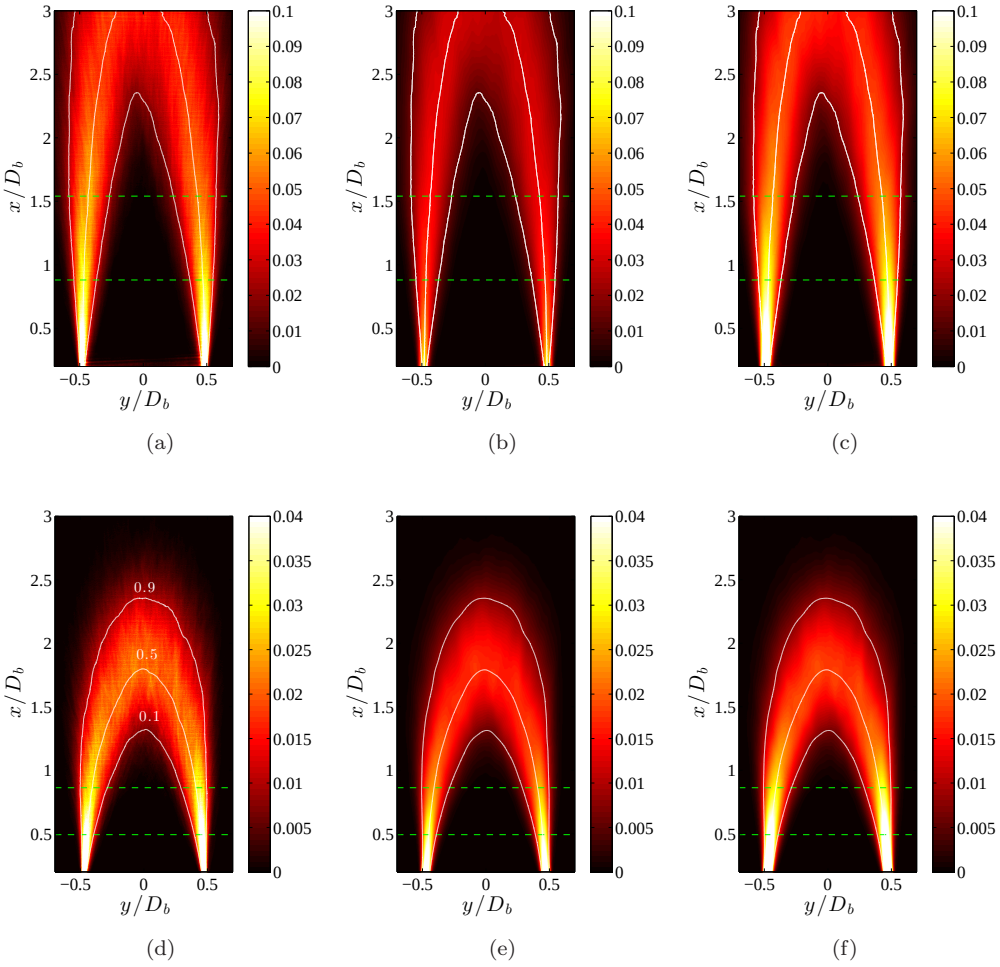

Figure 4. Maps of FSD normalized by δ_L. The streamwise x and transverse y coordinates are normalized by the burner diameter D_b. White curves represent three different iso-contours of progress variable $\langle c \rangle = 0.1$, 0.5, 0.9. The horizontal green dashed lines represent $x = 0.4H_f$ and $x = 0.7H_f$. Left : Total FSD $\langle |\nabla c| \rangle$, Center : Resolved FSD $\langle |\nabla \overline{c}| \rangle$ using a filter size of $16dx$, Right : Modeled FSD $\langle |\nabla \overline{c}| \rangle \Xi$ using a filter size of $16dx$. Top panel Ka^+, bottom panel Ka^-.

$\langle |\nabla c| \rangle$ and $\langle |\nabla \overline{c}| \rangle$ or equivalently that $\Xi_{2D} = \Xi_{3D}$. Given this assumption, only 2D flame surface density profiles will be displayed. Further work is though needed to confirm this statement.

2D plots of the measured, resolved and modeled FSD are presented in Fig. 4. A carefull analysis of Figs. 4(a) and 4(d) highlights that the flame height is much larger for case Ka^+ as compared to case Ka^-. This is attributed to a much smaller laminar flame speed S_L for case Ka^+ associated with both a higher pressure magnitude and a leaner equivalence ratio. The ratio of turbulent to laminar flame speed as inferred from the cone aera method (using the iso progress variable $\overline{c} = 5\%$) results in $S_T/S_L = 3.76$ for case Ka^+ and 1.65 for Ka^- indicating a much larger wrinkling of the flame for case Ka^+. Consistently, this difference in S_T/S_L is also observed on the magnitude of the flame surface density which is more than two times larger for case Ka^+ as compared to Ka^-. Also presented is the resolved (Figs 4(b) and 4(e)) and modeled (Figs 4(c) and 4(f)) FSD. For these figures, use was made of a filter size of $16dx$, which corresponds to 20 and 13 laminar flame thickness δ_L for case Ka^+ and Ka^- respectively. One notes that the FSD is more resolved for case Ka^- as compared to case Ka^+, highlighting again a much higher

SGS wrinkling for case Ka^+. In both case, the modeled FSD agree well with that measured, suggesting that the present model is reliable.

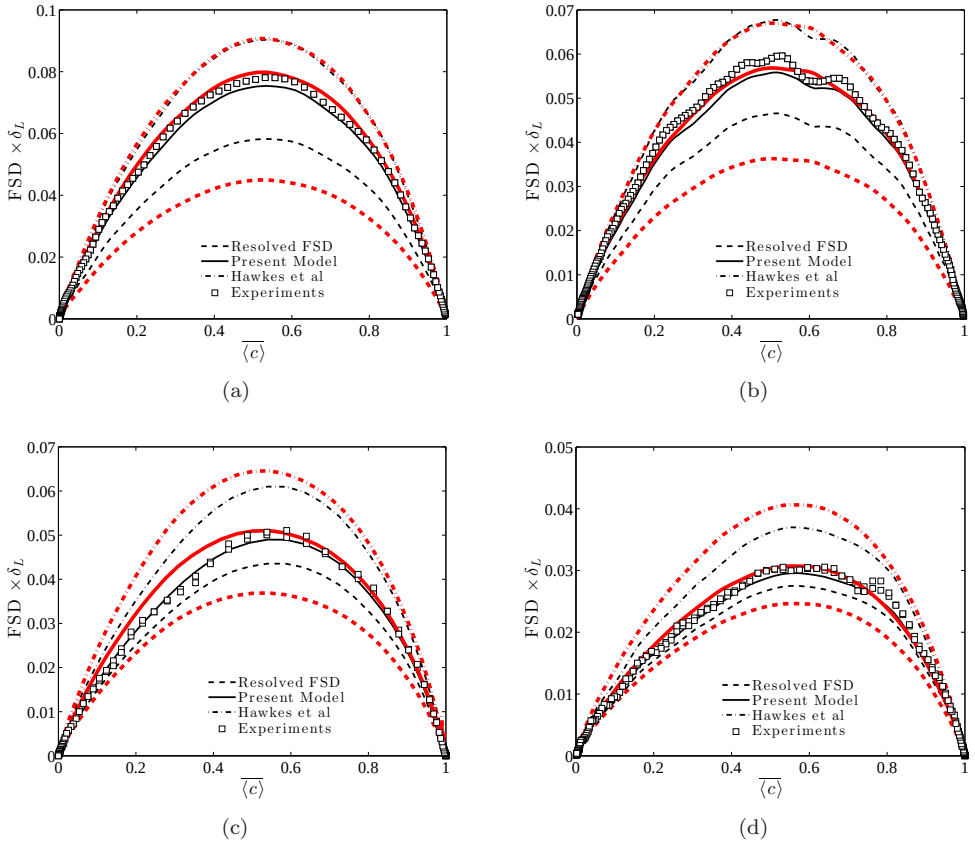

Figure 5. FSD as a function of the mean filtered progress variable $\langle \overline{c} \rangle$, for two distinct streamwise locations in the flow, (a,c) $x/H_f = 0.4$ and (b,d) $x/H_f = 0.7$ (the flame height H_f is defined as the location x where $\overline{c} = 5\%$). Top panel (a,b) is for the case Ka^+ and bottom panel (c,d) is for Ka^-. □ measured FSD, - - - resolved FSD, — present model $N = 1$, $a = 1$, $b = r_1^*$, $\eta_0 = 3L_t$ and $\alpha = 2$, – · – Hawkes et al. [16] model $N = 4$, $a = 0.2$, $b = 12.5$, $\eta_0 = \infty$ and $\alpha = 2$. The black curves corresponds to a filter size of $8dx$, whilst red curves to a filter size of $16dx$.

More quantitative results are further presented in Fig. 5 where the measured FSD is plotted as a function of the progress variable and compared to that resolved using a filter size of 8 and $16dx$ for two distinct streamwize locations, i.e $x/H_f = 0.4$ and $x/H_f = 0.7$ (denoted by the green dashed line in Fig. 4). The ratio of the filter size to laminar flame thickness is then 10 and 20 for case Ka^-, 6.5 and 13 for case Ka^+. Noticeable is the magnitude of the resolved FSD which is attenuated by about 25% and 50% for case Ka^+, when the filter size increases from $8dx$ to $16dx$. For case Ka^-, the resolved FSD represents about 82% and 70% of the total FSD when the filter size increases from $8dx$ to $16dx$. The present model yields very encouraging results since the reconstructed FSD agrees almost perfectly with that inferred from experiments, irrespectively of the filter size, streamwise distance, and Karlovitz number (Figs. 5(a), 5(b), 5(c) and 5(d)). Although results are not presented here, the models have been tested for other Karlovitz and Reynolds numbers, leading to similar deductions.

In Ref. [16], using *a priori* tests, the constants $N = 4$, $a = 0.3$, $b = 12.5$ and $\alpha = 1$ were found to be appropriate for modelling the SGS FSD of an hydrogen flame evolving in a highly turbulent plane jet. However, when compared to our experiments for the methane/air Bunsen flames, one notes slightly overestimated

values by about 10-15% depending on the location in the flow and Karlovitz number. This difference is most likely attributed to the difference in fuel composition (hydrogen vs methane), and especially to a non unity Lewis number effect that leads to a more wrinkled flame in the case of hydrogen flames. In addition, the flow configuration of Hawkes et al. [16] was a plane jet dominated by a very strong shear, which could also accentuate the wrinkling of the flame. In the Bunsen burner, these two effects are much less important thus explaining the observed overestimation of the SGS FSD when use is made of $N = 4$, $a = 0.3$, $b = 12.5$ and $\alpha = 1$.

4. Conclusion

In summary, six distinct outcomes emerge from the present study.

(i) An analytical expression for the efficiency function is proposed on the basis of some physical reasoning arguments. It accounts for viscous effects which dominates for Karlovitz numbers $Ka > 1$ as well as a kinematic constraint à la Peters [23] whose effect is dominant at low Karlovitz numbers. These two distinct regimes correspond respectively to the Damkhöler small and large-scale asymptotic limits. In the small-scale asymptotic limit, the flame front behaves as a passive scalar and the maximum effective stretch predicted by the present model is in close agreement with the value of 0.28 inferred by both Ref. [30] and Ref. [31].

(ii) The inner cut-off length-scale follows from the conjecture that η_i is the scale at which the active stretch rate is maximum. As a consequence of the definition of $\mathcal{C}$, η_i also reveals two different scalings with Karlovitz number corresponding to the two aforementioned regimes. It is then observed that at low Karlovitz number, the cut-off corresponds to the Gibson length-scale, as suggested by Peters[23], whilst at high Karlovitz numbers, the cut-off is the cross-over length-scale between viscous and inertial ranges (i.e. $r_1^* = (3C_q)^{3/4}$) in agreement with Ref. [39].

(iii) The present approach allows to estimate the constants a, b, N in the model of Ref. [16] on the basis of some physical arguments. It is thus proven that $a = 1$, $b = r_1^*$ and $N = 1$ are more suitable.

(iv) A new expression for the wrinkling factor (Eq. (11)) is introduced although not demonstrated, revealing the additional parameter η_0, related to the integral length scale to account for finite Reynolds number effects. This expression compares favourably well with the DNS results of Ref. [16] when a value of 2 is chosen for α in agreement with Ref. [25]. Future analytical work will address this specific relevance of this expression for Ξ.

(v) A careful analysis of Fig. 2(b) shows that in most of practical situations, the Reynolds number is not sufficiently large for a reliable value of the fractal dimension to be inferred. At finite Reynolds numbers, the estimation is biased, and the apparent fractal dimension systematically appears less steeper than the asymptotic value.

(vi) *A priori* tests are provided by comparing modeled FSDs to that measured in a lean methane-air Bunsen flame. Although further work is needed for testing the ability of this model using *a posteriori* tests, present results already give strong support in favour of the model.

Acknowledgements

The financial support from the Agence National de la Recherche under the project IDYLLE is gratefully acknowledged. We are also thankful to the CNRS, the

University of Orléans, and the French Government Program "Investissements d'avenir" through the LABEX CAPRYSSES. Denis Veynante from laboratory EM2C, Chatenay-Malabry is gratefully acknowledged for fruitfull discussions about an earlier version of this manuscript.

References

[1] T. Poinsot and D. Veynante, *Theoretical and numerical combustion*, RT Edwards, Inc., 2005.
[2] O. Colin, F. Ducros, D. Veynante, and T. Poinsot, *A thickened flame model for large eddy simulations of turbulent premixed combustion*, Phys. Fluids 12 (2000), pp. 1843–1863.
[3] F. Charlette, C. Meneveau, and D. Veynante, *A power-law flame wrinkling model for LES of premixed turbulent combustion part I: non-dynamic formulation and initial tests*, Combust. Flame 131 (2002), pp. 159–180.
[4] H. Pitsch and L. Duchamp de Lageneste, *Large-eddy simulation of premixed turbulent combustion using a level-set approach*, Proc. Combust. Inst. 29 (2002), pp. 2001–2008.
[5] H. Pitsch, *A consistent level set formulation for large-eddy simulation of premixed turbulent combustion*, Combust. Flame 143 (2005), pp. 587–598.
[6] B. Fiorina, R. Vicquelin, P. Auzillon, N. Darabiha, O. Gicquel, and D. Veynante, *A filtered tabulated chemistry model for LES of premixed combustion*, Combust. Flame 157 (2010), pp. 465–475.
[7] C. Meneveau and T. Poinsot, *Stretching and quenching of flamelets in premixed turbulent combustion*, Combust. Flame 86 (1991), pp. 311–332.
[8] S. Bougrine, S. Richard, O. Colin, and D. Veynante, *Fuel composition effects on flame stretch in turbulent premixed combustion: Numerical analysis of flame-vortex interaction and formulation of a new efficiency function*, Flow, Turb. and Combust. 93 (2014), pp. 259–281.
[9] T. Poinsot, D. Veynante, and S. Candel, *Quenching processes and premixed turbulent combustion diagrams*, J. Fluid Mech. 228 (1991), pp. 561–606.
[10] T. Poinsot, D. Veynante, and S. Candel, *Diagrams of premixed turbulent combustion based on direct simulation*, Symposium (International) on Combustion 23 (1991), pp. 613–619.
[11] H. Tennekes and J.L. Lumley, *A first course in turbulence*, MIT press, 1972.
[12] H. Tennekes, *Eulerian and lagrangian time microscales in isotropic turbulence*, J. Fluid Mech. 67 (1975), pp. 561–567.
[13] W.L. Roberts and J.F. Driscoll, *A laminar vortex interacting with a premixed flame: measured formation of pockets of reactants*, Combust. Flame 87 (1991), pp. 245–256.
[14] N. Malik and J. Vassilicos, *Eulerian and lagrangian scaling properties of randomly advected vortex tubes*, J. Fluid Mech. 326 (1996), pp. 417–436.
[15] C. Poulain, N. Mazellier, L. Chevillard, Y. Gagne, and C. Baudet, *Dynamics of spatial fourier modes in turbulence*, The European Physical Journal B 53 (2006), pp. 219–224.
[16] E.R. Hawkes, O. Chatakonda, H. Kolla, A.R. Kerstein, and J.H. Chen, *A petascale direct numerical simulation study of the modelling of flame wrinkling for large-eddy simulations in intense turbulence*, Combust. Flame 159 (2012), pp. 2690–2703.
[17] C. Angelberger, D. Veynante, F. Egolfopoulos, and T. Poinsot, *Large eddy simulations of combustion instabilities in premixed flames*, in *Proc. of the Summer Program*, Available at http://ctr.stanford.edu/ctrsp98/angelberger.pdf, 1998, pp. 61–82.
[18] C. Fureby, *A fractal flame-wrinkling large eddy simulation model for premixed turbulent combustion*, Proc. Combust. Inst. 30 (2005), pp. 593–601.
[19] F. Thiesset, L. Danaila, and R.A. Antonia, *Dynamical effect of the total strain induced by the coherent motion on local isotropy in a wake.*, J. Fluid Mech. 720 (2013), pp. 393–423.
[20] T. Kármán and L. Howarth, *On the statistical theory of isotropic turbulence*, Proc. Roy. Soc. Lond. A 164 (917) (1938), pp. 192–215, Available at http://www.jstor.org/stable/97087.
[21] A. Kolmogorov, *Dissipation of energy in the locally isotropic turbulence*, Dokl. Akad. Nauk. SSSR 125 (1941), pp. 15–17.
[22] L. Danaila, R.A. Antonia, and P. Burattini, *Progress in studying small-scale turbulence using 'exact' two-point equations*, New J. Phys. 6 (2004), p. 128.
[23] N. Peters, *Laminar flamelet concepts in turbulent combustion*, Symposium (International) on Combustion 21 (1986), pp. 1231–1250.
[24] R.A. Antonia, R.J. Smalley, T. Zhou, F. Anselmet, and L. Danaila, *Similarity of energy structure functions in decaying homogeneous isotropic turbulence*, J. Fluid Mech. 487 (2003), pp. 245–269.

[25] G.K. Batchelor, *Pressure fluctuations in isotropic turbulence*, Proc. Camb. Phi. Soc. 47 (1951), pp. 359–374.
[26] S. Kurien and K.R. Sreenivasan, *Anisotropic scaling contributions to high-order structure functions in high-Reynolds-number turbulence.*, Phys. Rev. E 62 (2000), pp. 2206–2212.
[27] K.G. Aivalis, K.R. Sreenivasan, Y. Tsuji, J. Klewicki, and C.A. Biltoft, *Temperature structure functions for air flow over moderately heated ground*, Phys. Fluids 14 (2002), pp. 2439–2446.
[28] S.B. Pope, *Turbulent flows*, Cambridge university press, 2000.
[29] Y.H. Pao, *Structure of turbulent velocity and scalar fields at large wavenumbers*, Phys. Fluids 8 (1965), pp. 1063–1075.
[30] P. Yeung, S. Girimaji, and S. Pope, *Straining and scalar dissipation on material surfaces in turbulence: implications for flamelets*, Combust. Flame 79 (1990), pp. 340–365.
[31] S. Goto and S. Kida, *Reynolds-number dependence of line and surface stretching in turbulence: folding effects*, J. Fluid Mech. 586 (2007), pp. 59–81.
[32] F. Gouldin, S. Hilton, and T. Lamb, *Experimental evaluation of the fractal geometry of flamelets*, Symposium (International) on Combustion 22 (1989), pp. 541–550.
[33] G. North and D. Santavicca, *The fractal nature of premixed turbulent flames*, Combust. Sci. Technol. 72 (1990), pp. 215–232.
[34] O. Chatakonda, E.R. Hawkes, A.J. Aspden, A.R. Kerstein, H. Kolla, and J.H. Chen, *On the fractal characteristics of low Damköhler number flames*, Combust. Flame 160 (2013), pp. 2422–2433.
[35] F. Gouldin, *An application of fractals to modeling premixed turbulent flames*, Combust. Flame 68 (1987), pp. 249–266.
[36] A.R. Kerstein, *Fractal dimension of turbulent premixed flames*, Combust. Sci. Technol. 60 (1988), pp. 441–445.
[37] N. Peters and C. Franke, *The fractal concept of turbulent flames*, in *Dissipative Structures in Transport Processes and Combustion*, Springer, 1990, pp. 40–50.
[38] G. Batchelor, *The effect of homogeneous turbulence on material lines and surfaces*, Proc. Roy. Soc. Lond. A 213 (1952), pp. 349–366.
[39] H. Kobayashi, T. Kawahata, K. Seyama, T. Fujimari, and J.S. Kim, *Relationship between the smallest scale of flame wrinkles and turbulence characteristics of high-pressure, high-temperature turbulent premixed flames*, Proc. Combust. Inst. 29 (2002), pp. 1793–1800.
[40] S. Menon and A.R. Kerstein, *Stochastic simulation of the structure and propagation rate of turbulent premixed flames*, Symposium (International) on Combustion 24 (1992), pp. 443–450.
[41] R. Fragner, N. Mazellier, F. Halter, C. Chauveau, and I. Gökalp, *Multi scale high intensity turbulence generator applied to a high pressure turbulent burner*, Flow, Turb. and Combust. 94(1) (2014), pp. 1–21.
[42] R. Fragner, F. Halter, N. Mazellier, C. Chauveau, and I. Gökalp, *Investigation of pressure effects on the small scale wrinkling of turbulent premixed bunsen flames*, Proc. Combust. Inst. 35(2) (2015), pp. 1527–1535.
[43] R.J. Kee, J.F. Grcar, M. Smooke, J. Miller, and E. Meeks, *PREMIX: a fortran program for modeling steady laminar one-dimensional premixed flames*, Sandia National Laboratories Report (1985).
[44] R.J. Kee, F.M. Rupley, and J.A. Miller, *The chemkin thermodynamic data base*, Tech. Rep., Sandia National Labs., Livermore, CA (USA), 1990.
[45] G. Smith, D. Golden, M. Frenklach, N. Moriarty, B. Eiteneer, M. Goldenberg, C. Bowman, R. Hanson, S. Song, W. Gardiner, *et al.*, *Gri-mechan optimized detailed chemical reaction mechanism for methane combustion*, Tech. Rep., Technical Report http://www. me. berkeley. edu/gri mech, Gas Research Institute, 1999.
[46] E.R. Hawkes, R. Sankaran, and J.H. Chen, *Estimates of the three-dimensional flame surface density and every term in its transport equation from two-dimensional measurements*, Proc. Combust. Inst. 33 (2011), pp. 1447–1454.
[47] F. Halter, C. Chauveau, I. Gökalp, and D. Veynante, *Analysis of flame surface density measurements in turbulent premixed combustion*, Combust. Flame 156 (2009), pp. 657–664.
[48] D. Veynante, G. Lodato, P. Domingo, L. Vervisch, and E.R. Hawkes, *Estimation of three-dimensional flame surface densities from planar images in turbulent premixed combustion*, Exp. in Fluids 49 (2010), pp. 267–278.
[49] N. Chakraborty and E.R. Hawkes, *Determination of 3D flame surface density variables from 2D measurements: Validation using direct numerical simulation*, Phys. Fluids 23 (2011), p. 065113.